Attribution of growing season evapotranspiration variability considering snowmelt and vegetation changes in the arid alpine basins

Tingting Ning[abc], Zhi Li[d], Qi Feng[ac]* , Zongxing Li[ac] and Yanyan Qin[b]

[a]*Key Laboratory of Ecohydrology of Inland River Basin, Northwest Institute of Eco-Environment and Resources, Chinese Academy of Sciences, Lanzhou, 730000, China*

[b]*Key Laboratory of Land Surface Process and Climate Change in Cold and Arid Regions, Chinese Academy of Sciences, Lanzhou 730000, China*

[c]*Qilian Mountains Eco-environment Research Center in Gansu Province, Lanzhou, 730000, China*

[d]*College of Natural Resources and Environment, Northwest A&F University, Yangling, Shaanxi, 712100, China*

* Correspondence to: Qi Feng (qifeng@lzb.ac.cn)

Abstract: Previous studies have successfully applied variance decomposition frameworks based on the Budyko equations to determine the relative contribution of variability in precipitation, potential evapotranspiration (E_0), and total water storage changes (ΔS) to evapotranspiration variance (σ_{ET}^2) on different time-scales; however, the effects of snowmelt (Q_m) and vegetation (M) changes have not been incorporated into this framework in snow-dependent basins. Taking the arid alpine basins in the Qilian Mountains in northwest China as the study area, we extended the Budyko framework to decompose the growing season σ_{ET}^2 into the temporal variance and covariance of rainfall (R), E_0, ΔS, Q_m, and M. The results indicate that the incorporation of Q_m could improve the performance of the Budyko framework on a monthly scale; σ_{ET}^2 was primarily controlled by the R variance with a mean contribution of 63%, followed by the coupled R and M (24.3%) and then the coupled R and E_0 (14.1%). The effects of M variance or Q_m variance cannot be ignored because they contribute to 4.3% and 1.8% of σ_{ET}^2, respectively. By contrast, the interaction of some coupled factors adversely affected σ_{ET}^2, and the 'out-of-phase' seasonality between R and Q_m had the largest effect (−7.6%). Our methodology and these findings are helpful for quantitatively assessing and understanding hydrological responses to climate and vegetation changes in snow-dependent regions on a finer time-scale.

Keywords: evapotranspiration variability; snowmelt; vegetation; attribution

1 Introduction

Actual evapotranspiration (*ET*) drives energy and water exchanges among the hydrosphere, atmosphere, and biosphere (Wang et al., 2007). The temporal variability in *ET* is, thus, the combined effect of multiple factors interacting across the soil–vegetation–atmosphere interface (Katul et al., 2012; Xu and Singh, 2005). Investigating the mechanism behind *ET* variability is also fundamental for understanding hydrological processes. The basin-scale *ET* variability has been widely investigated with the Budyko framework (Budyko, 1961, 1974); however, most studies are conducted on long-term or inter-annual scales and cannot interpret the short-term *ET* variability (e.g. monthly scales).

Short-term *ET* and runoff (Q_r) variance have been investigated recently for their dominant driving factors (Feng et al., 2020; Liu et al., 2019; Wu et al., 2017; Ye et al., 2016; Zeng and Cai, 2015; Zeng and Cai, 2016; Zhang et al., 2016a); to this end, an overall framework was presented by Zeng and Cai (2015) and Liu et al. (2019). Zeng and Cai (2015) decomposed the intra-annual *ET* variance into the variance/covariance of precipitation (P), potential evapotranspiration (E_0), and water storage change (ΔS) under the Budyko framework based on the work of Koster and Suarez (1999). Subsequently, Liu et al. (2019) proposed a new framework to identify the driving factors of global Q_r variance by considering the temporal variance of P, E_0, ΔS, and other factors such as the climate seasonality, land cover, and human impact. Although the proposed framework performs well for the ET variance decomposition, further research is necessary for considering additional driving factors and for studying regions with unique hydrological processes.

The impact of vegetation change should first be fully considered when studying the variability of ET. Vegetation change significantly affects the hydrological cycle through rainfall interception, evapotranspiration, and infiltration (Rodriguez-Iturbe, 2000; Zhang et al., 2016b). Higher vegetation coverage increases ET and reduces the ratio of Q_r to P (Feng et al., 2016). However, most of the existing studies on ET variance decomposition either ignored the effects of vegetation change or did not quantify its contributions. Vegetation change is closely related to the Budyko controlling parameters, and several empirical relationships have been successfully developed on long-term and inter-annual scales (Li et al., 2013; Liu et al., 2018; Ning et al., 2020; Xu et al., 2013; Yang et al., 2009). However, the relationship between vegetation and its controlling parameters on a finer time-scale has received less attention. As such, it is important to quantitatively investigate the contribution of vegetation change to ET variability on a finer time-scale.

Second, for snow-dependent regions, the short-term water balance equation was the foundation of decomposing ET/or Q_r variance. Its general form can be expressed as:

$$P = ET + Q_r + \Delta S, \tag{1}$$

where P, including liquid (rainfall) and solid (snowfall) precipitation, is the total water source of the hydrological cycle. But this equation is unsuitable for regions where the land-surface hydrology is highly dependent on the winter mountain snowpack and spring snowmelt runoff. It has been reported that annual Q_r originating from snowmelt accounts for 20–70% of the total runoff, including west United States (Huning and AghaKouchak, 2018), coastal areas of Europe (Barnett et al., 2005), west China (Li et al., 2019b), northwest India (Maurya et al., 2018), south of the Hindu Kush (Ragettli et al., 2015), and high-mountain Asia (Qin et al., 2020). In these regions, the mountain snowpack serves as a natural reservoir that stores cold-season P to meet the warm-season water demand (Qin et al., 2020; Stewart, 2009). Thus, the water balance equation should be modified to consider the impacts of snowmelt on runoff in short-term time scale:

$$R + Q_m = ET + Q_r + \Delta S, \tag{2}$$

where R is the rainfall, and Q_m is the snowmelt runoff. Many observations and modelling experiments have found that due to global warming, increasing temperatures would induce earlier runoff in the spring or winter and reduce the flows in summer and autumn (Barnett et al., 2005; Godsey et al., 2014; Stewart et al., 2005; Zhang et al., 2015). Therefore, the role of snowmelt change on ET variability in snow-dependent basins on a finer time-scale should be studied.

The overall objective of this study was to decompose the *ET* variance into the temporal variability of multiple factors considering vegetation and snowmelt change. The six cold alpine basins in the Qilian Mountains of northwest China were taken as an example study area. Specifically, we aimed to: (i) determine the dominant driving factor controlling the *ET* variance; (2) investigate the roles of vegetation and snowmelt change in the variance; and (3) understand the interactions among the controlling factors in *ET* variance. The proposed method will help quantify the hydrological response to changes in snowmelt and vegetation in snowmelt-dependent regions, and our results will prove to be insightful for water resource management in other similar regions worldwide.

2 Materials

2.1 Study area

Six sub-basins located in the upper reaches of the Heihe, Shiyang, and Shule rivers in the Qilian Mountains were chosen as the study area (Figure 1). They are important inland rivers in the dry region of northwest China. The runoff generated from the upper reaches contributes to nearly 70% of the water resources of the entire basin and thus plays an important role in supporting agriculture, industry development, and ecosystem maintenance in the middle and downstream rivers (Cong et al., 2017; Wang et al., 2010a). Snowmelt and in-mountain-generated rainfall make up the water supply system for the upper basins (Matin and Bourque, 2015), and the annual average *P* exceeds 450 mm in this region. At higher altitudes, as much as 600–700 mm of P can be observed (Yang et al., 2017). Nearly 70% of the total rainfall concentrates between June and September, while only 19% of the total rainfall occurs from March to June. Snowmelt runoff is an important water source (Li et al., 2012; Li et al., 2018; Li et al., 2016); in the spring, 70% of the runoff is supplied by snowmelt water (Wang and Li, 2001). Characterised by a continental alpine semi-humid climate, alpine desert glaciers, alpine meadows, forests, and upland meadows are the predominant vegetation distribution patterns (Deng et al., 2013). Furthermore, this region has experienced substantial vegetation changes and resultant hydrological changes in recent decades (Bourque and Mir, 2012; Du et al., 2019; Ma et al., 2008).

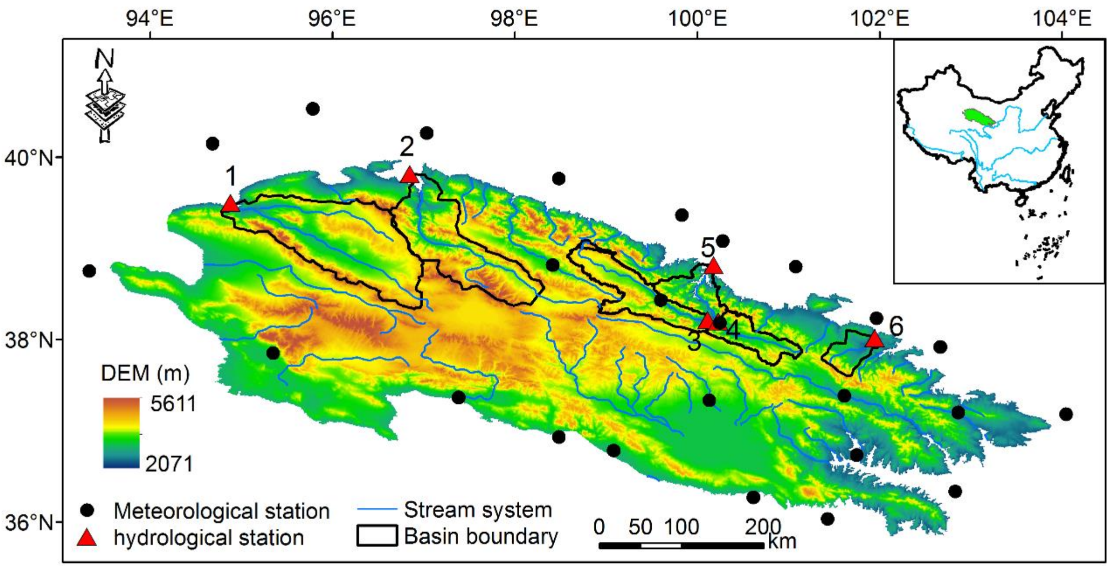

Figure 1 The six basins in China’s northern Qilian Mountains. The Digital elevation data, at 30 m resolution, was provided by the Geospatial Data Cloud site, Computer Network Information Center, Chinese Academy of Sciences.

2.2 Data

Daily climate data were collected for 25 stations distributed in and around the Qilian Mountains from the China Meteorological Administration. They comprised rainfall, air temperature, sunshine hours, and relative humidity and would be used to calculate the monthly E_0 using the Priestley and Taylor (1972) equation.

The monthly runoff at the Dangchengwan, Changmabu, Zhamashike, Qilian, Yingluoxia, and Shagousi hydrological stations were obtained for 2001–2014 from the Bureau of Hydrology and Water Resources, Gansu Province. The sum of the monthly soil moisture and plant canopy surface water with a resolution of 0.25° × 0.25° from the Global Land Data Assimilation System (GLDAS) Noah model was used to estimate the total water storage. The monthly ΔS was calculated as the water storage difference between two neighbouring months. Eight-day composites of the MODIS MOD10A2 Version 6 snow cover product from the MODIS TERRA satellite were used to produce the monthly snow cover area (*SCA*) of each basin. The *SCA* data were used to drive the snowmelt runoff model.

A monthly normalised difference vegetation index (*NDVI*) at a spatial resolution of 1 km from the MODIS MOD13A3.006 product was used to assess the vegetation coverage (*M*), which can be calculated from the method of Yang et al. (2009):

$$M = \frac{NDVI - NDVI_{min}}{NDVI_{max} - NDVI_{min}} \tag{3}$$

where $NDVI_{max}$ and $NDVI_{min}$ are the $NDVI$ values of dense forest (0.80) and bare soil (0.05).

ET from dataset of "ground truth of land surface evapotranspiration at regional scale in the Heihe River Basin (2012-2016) $\mathrm{ET_{map}}$ Version 1.0" (hereafter "ET_{map}"), was used to validate the reliability of our estimated ET. This dataset was published by National Tibetan Plateau Data Center. It was upscaled from 36 eddy covariance flux tower sites (65 site years) to the regional scale with five machine learning algorithms, and then applied to estimate ET for each grid cell (1 km × 1 km) across the Heihe River Basin each day from May to September over the period 2012–2016. It has been evaluated to have high accuracy (Xu et al., 2018). Basins 3,4,5 in our study belongs to the headwater sub-basins of Heihe River, and our monthly ET from May to September during 2012-2014 was thus compared with ET_{map}.

3 Methods

3.1 The Budyko framework at monthly scales

Probing the ET variability in the growing season can provide basic scientific reference points for agricultural activities and water resource planning and management (Li et al., 2015; Wagle and Kakani, 2014). Thus, we focus on the growing season ET variability on a monthly scale in this study.

Among the mathematical forms of the Budyko framework, this study employed the function proposed by Choudhury (1999) and Yang et al. (2008) to assess the basin water balance for good performance (Zhou et al., 2015):

$$ET = \frac{P_e \times E_0}{({P_e}^n + E_0^n)^{1/n}}, \tag{4}$$

where n is the controlling parameter of the Choudhury–Yang equation. P_e is the total available water supply for ET. In previous studies, P_e included P and ΔS (P_e=P-ΔS) on finer time scale (Liu et al., 2019; Zeng and Cai, 2015; Zhang et al., 2016a). But snowmelt runoff should also be considered in the snow-dependent basins. Thus, P_e can be defined as:

$$P_e = R + Q_S - \Delta S. \tag{5}$$

Equation 4 can thus be redefined as follows:

$$ET_i = \frac{(R_i + Q_{S_i} - \Delta S_i) \times E_{0_i}}{((R_i + Q_{S_i} - \Delta S_i)^{n_i} + E_{0_i}^{n_i})^{1/n_i}}, \tag{6}$$

where i indicates each month of the growing season (April to September). After estimating the monthly ET of the growing season using Equation 2, the values of n for each month can be obtained via Equation 6.

3.2 Estimating the equivalent of snowmelt runoff

With the developed relationship between snowmelt and air temperature (Hock, 2003), the degree-day model simplifies the complex processes and performs well, so it is widely used in snowmelt estimation (Griessinger et al., 2016; Rice et al., 2011; Semadeni-Davies, 1997; Wang et al., 2010a). This study estimated the monthly Q_s using the degree-day model following the Wang et al. (2015) procedure. Specifically, the water equivalent of snowmelt (*W*, mm) during the period *m* can be calculated as:

$$\sum_{i=1}^{m} W_i = DDF \sum_{i=1}^{m} T_i^+, \tag{7}$$

where *DDF* denotes the degree-day factor (mm/day · ° C), and T^+ is the sum of the positive air temperatures of each month. After obtaining *W*, the monthly Q_s of each elevation zone can be expressed as:

$$\sum_{i=1}^{m} Q_{Si} = \sum_{i=1}^{m} W_i \, SCA_i, \tag{8}$$

where SCA_i is the snow cover area of each elevation zone.

According to Gao et al. (2011), the *DDF* values of Basins 1–6 were set to 3.4, 3.4, 4.0, 4.0, 4.0, and 1.7 mm/day · °C, respectively. The six basins were divided into seven elevation zones with elevation differences of 500 m. The sum of Q_s in each elevation zone could be considered as the total Q_s of each basin. Previous studies have found that the major snow melting period is from March to July in this area (Wang and Li, 2005; Wu et al., 2015); furthermore, the MODIS snow product also showed that the *SCA* decreased significantly at the end of July. Thus, the snowmelt runoff from April to July for the growing season was estimated in this study.

3.3 Relationship between the Budyko controlling parameter and vegetation change

The relationships between the monthly parameters n and M for each basin in the growing season for 2001–2014 are presented in Figure 2. It can be seen that parameter n was significantly positively related to M in all six basins ($p < 0.05$), which means that ET increased with increasing vegetation conditions under the given climate conditions.

In Equation 6, when $n \rightarrow 0$, $ET \rightarrow 0$, which means M should have the following limiting conditions: if $ET \rightarrow 0$, $T \rightarrow 0$ (transpiration), and thus $M \rightarrow 0$. Considering the relationship shown in Figure 2 and the above limiting conditions, the general form of parameter n can be expressed by power function followed previous studies (Liu et al., 2018; Ning et al., 2017; Yang et al., 2007):

$$n = a \times M^{b}, \tag{9}$$

where a and b are constants, and their specific values for each basin are fitted in Figure 2.

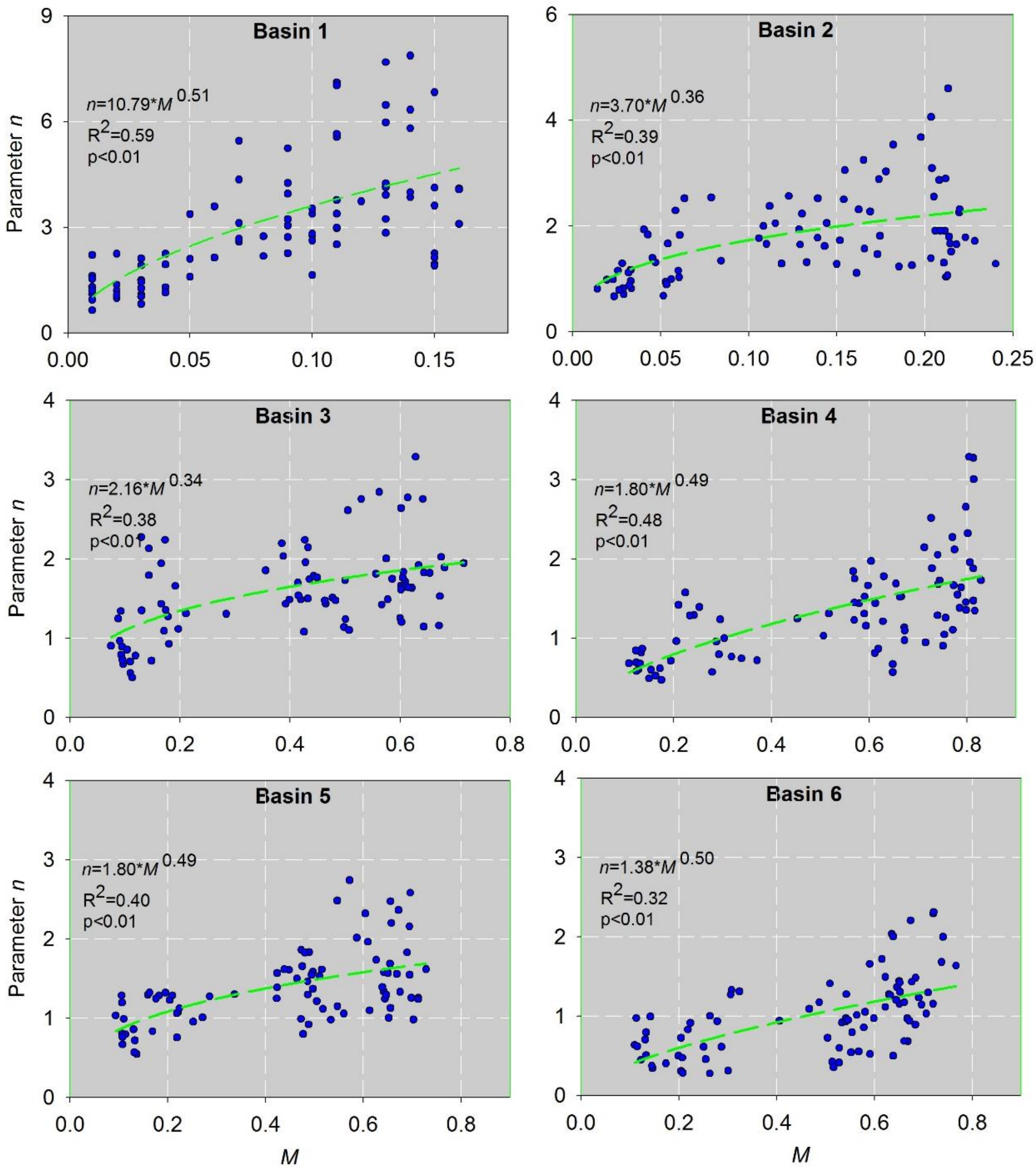

Figure 2 Relationships between the parameter *n* and the vegetation coverage for each basin on a monthly scale.

3.4 *ET* variance decomposition

Liu et al. (2019) proposed a framework to identify the driving factors behind the temporal variance of Q_r by combining the unbiased sample variance of Q_r with the total differentiation of Q_r changes. Here, we extended this method by considering the effects of changes in snowmelt runoff and vegetation coverage on ET variance.

By combining Equation 6 with Equation 9, Equation 6 can be simplified as $ET \approx f(R_i, Q_{mi}, \Delta S_i, E_{0i}, M_i)$. Thus, the total differentiation of ET changes can be expressed as:

$$dET_i = \frac{\partial f}{\partial R} dR_i + \frac{\partial f}{\partial Q_s} dQ_{m_i} + \frac{\partial f}{\partial \Delta S} d\Delta S_i + \frac{\partial f}{\partial E_0} dE_{0_i} + \frac{\partial f}{\partial M} dM_i + \tau, \quad (10)$$

where τ is the error. $\frac{\partial f}{\partial R}$, $\frac{\partial f}{\partial Q_m}$, $\frac{\partial f}{\partial \Delta S}$, $\frac{\partial f}{\partial E_0}$, $\frac{\partial f}{\partial M}$ are the partial differential coefficients of ET to R, Q_m, ΔS, E_0 and M , respectively, which can be calculated as:

$$\frac{\partial ET}{\partial R} = \frac{\partial ET}{\partial Q_m} = -\frac{\partial ET}{\partial \Delta S} = \frac{ET}{P_e} \times \left(\frac{E_0^n}{P_e^n + E_0^n}\right), \quad (11a)$$

$$\frac{\partial ET}{\partial E_0} = \frac{ET}{E_0} \times \left(\frac{P_e^n}{P_e^n + E_0^n}\right), \quad (11b)$$

$$\frac{\partial ET}{\partial M} = \frac{ET}{n} \left(\frac{\ln (P_e^n + E_0^n)}{n} - \frac{P_e^n lnP + E_0^n lnE_0}{P_e^n + E_0^n}\right) \times a \times b \times M^{b-1}. \quad (11c)$$

The first-order approximation of ET changes in Equation 10 can be expressed as:

$$\Delta ET_i \approx \varepsilon_1 \Delta R_i + \varepsilon_2 \Delta Q_{s_i} + \varepsilon_3 \Delta S_i + \varepsilon_4 \Delta E_{0_i} + \varepsilon_5 \Delta M_i, \quad (12)$$

where $\varepsilon_1 = \frac{\partial ET}{\partial R}$; $\varepsilon_2 = \frac{\partial ET}{\partial Q_s}$; $\varepsilon_3 = \frac{\partial ET}{\partial \Delta S}$; $\varepsilon_4 = \frac{\partial ET}{\partial E_0}$; $\varepsilon_5 = \frac{\partial ET}{\partial M}$.

In this study, the temporal variance of ET reflects the fluctuation of monthly ET in growing season for years, which can be quantified by the unbiased sample variance (σ_{ET}^2) :

$$\sigma_{ET}^2 = \frac{1}{N-1}\sum_{i=1}^{N}(ET_i - \overline{ET})^2 = \frac{1}{N-1}\sum_{i=1}^{N}(\Delta ET_i)^2. \tag{13}$$

where $\overline{ET}$ is the long term monthly mean of *ET*. *N* is the sample size, it equals 84 in this study (6 months/year×14 years=84 months). *i* is used to index time series of month from 1 to *N*. σ_{ET}^2 indicates how far a set of monthly *ET* in growing season is spread out from their average value. The larger σ_{ET}^2, the larger fluctuation of *ET*, and vice versa.

Combining Equation 12 with Equation 13, σ_{ET}^2 can be decomposed as the contribution from different variance/covariance sources:

$$\sigma_{ET}^2 = \sum_{i=1}^{N}(\varepsilon_1\Delta R_i + \varepsilon_2\Delta Q_{s_i} + \varepsilon_3\Delta S_i + \varepsilon_4\Delta E_{0_i} + \varepsilon_5\Delta M_i)^2. \tag{14}$$

Expanding Equation 14, σ_{ET}^2 can be further rewritten as:

$$\sigma_{ET}^2 = \varepsilon_1^2\sigma_R^2 + \varepsilon_2^2\sigma_{Q_s}^2 + \varepsilon_3^2\sigma_{\Delta S}^2 + \varepsilon_4^2\sigma_{E_0}^2 + \varepsilon_5^2\sigma_M^2 + 2\varepsilon_1\varepsilon_2\mathrm{cov}(R, Q_s) + 2\varepsilon_1\varepsilon_3\mathrm{cov}(R, \Delta S) + 2\varepsilon_1\varepsilon_4\mathrm{cov}(R, E_0) + 2\varepsilon_1\varepsilon_5\mathrm{cov}(R, M) + 2\varepsilon_2\varepsilon_3\mathrm{cov}(Q_s, \Delta S) + 2\varepsilon_2\varepsilon_4\mathrm{cov}(Q_s, E_0) + 2\varepsilon_2\varepsilon_5\mathrm{cov}(Q_s, M) + 2\varepsilon_3\varepsilon_4\mathrm{cov}(E_0, \Delta S) + 2\varepsilon_3\varepsilon_5\mathrm{cov}(M, \Delta S) + 2\varepsilon_4\varepsilon_5\mathrm{cov}(E_0, M), \tag{15}$$

where *σ* represents the standard deviation, and *cov* represents the covariance. Equation 15 can be further simplified as:

$$\sigma_{ET}^2 = F(R) + F(Q_s) + F(\Delta S) + F(E_0) + F(M) + F(R\_Q_s) + F(R\_\Delta S) +$$

$$F(R\_E_0) + F(R\_M) + F(Q_s\_\Delta S) + F(Q_s\_E_0) + F(Q_s\_M) + F(\Delta S\_E_0) + F(\Delta S\_M) + F(E_0\_M), \quad (16)$$

Where F is the individual contributions of each factor; each two factors linked by underscore represents the interaction effects between them.

By separating out Equation 16, the contribution of each factor to σ_{ET}^2 can be calculated as:

$$C(X_{\mathrm{j}}) = \frac{F(X_j)}{\sigma_{ET}^2} \times 100\%, \quad (17)$$

where $C(X_{\mathrm{j}})$ is the contribution of factor $F(j)$ to σ_{ET}^2, and j = 1–15, representing the 15 factors in Equation 16.

4 Results and Discussion

4.1 The effects of monthly storage change and snowmelt runoff in the Budyko framework

The Budyko framework is usually used for analyses of long-term average catchment water balance; however, it was employed for the interpretation of the monthly variability of the water balance in this study. Thus, it’s very necessary to validate the feasibility of Budyko equation for monthly variability. Furthermore, the impact of ΔS on the representation of Budyko framework on a finer time-scale has been assessed by several studies (Chen et al., 2013; Du et al., 2016; Liu et al., 2019; Zeng and Cai, 2015). However, the impact of Q_m and its combined effects with ΔS in snowmelt-dependent basins are mostly ignored. Therefore, we present the water balance in the monthly scale of six basins in the Budyko's framework with three different computations of aridity index ($\phi=E_0/P_e$) or ET ratio (ET/P_e) in Figure 3. In Figure 3a, $ET=R\text{-}Q_r$ when R is considered as water supply, i.e., $P_e=R$. The points of monthly ET ratio and aridity index in April and May were well below Budyko curves in 6 basins; monthly ET ratio was even negative in several year, which means the local rain are not the only sources of ET in this area, especially in spring. In Figure 3b, $ET=R\text{-}\Delta S\text{-}Q_r$ with $P_e=R\text{-}\Delta S$. Compared with figure 3a, the way-off points in April and May were improved to a certain extent but negative points still existed, suggesting that except for R, ΔS also play a significant role in maintaining spring ET, but the variability of ET cannot be completely explained by these two variables. In Figure 3c, $ET=R\text{-}\Delta S+Q_m\text{-}Q_r$ with $Pe=R\text{-}\Delta S+Q_m$. Compared to the points in Figures 3a-b, all points focused on Budyko's curves more closely in each basin when $Pe=R+Q_m\text{-}\Delta S$. From this comparison, it can be concluded that the Budyko framework is applicable to the monthly scale in snowmelt-dependent basins, if the water supply is described accurately by considering ΔS and Q_m.

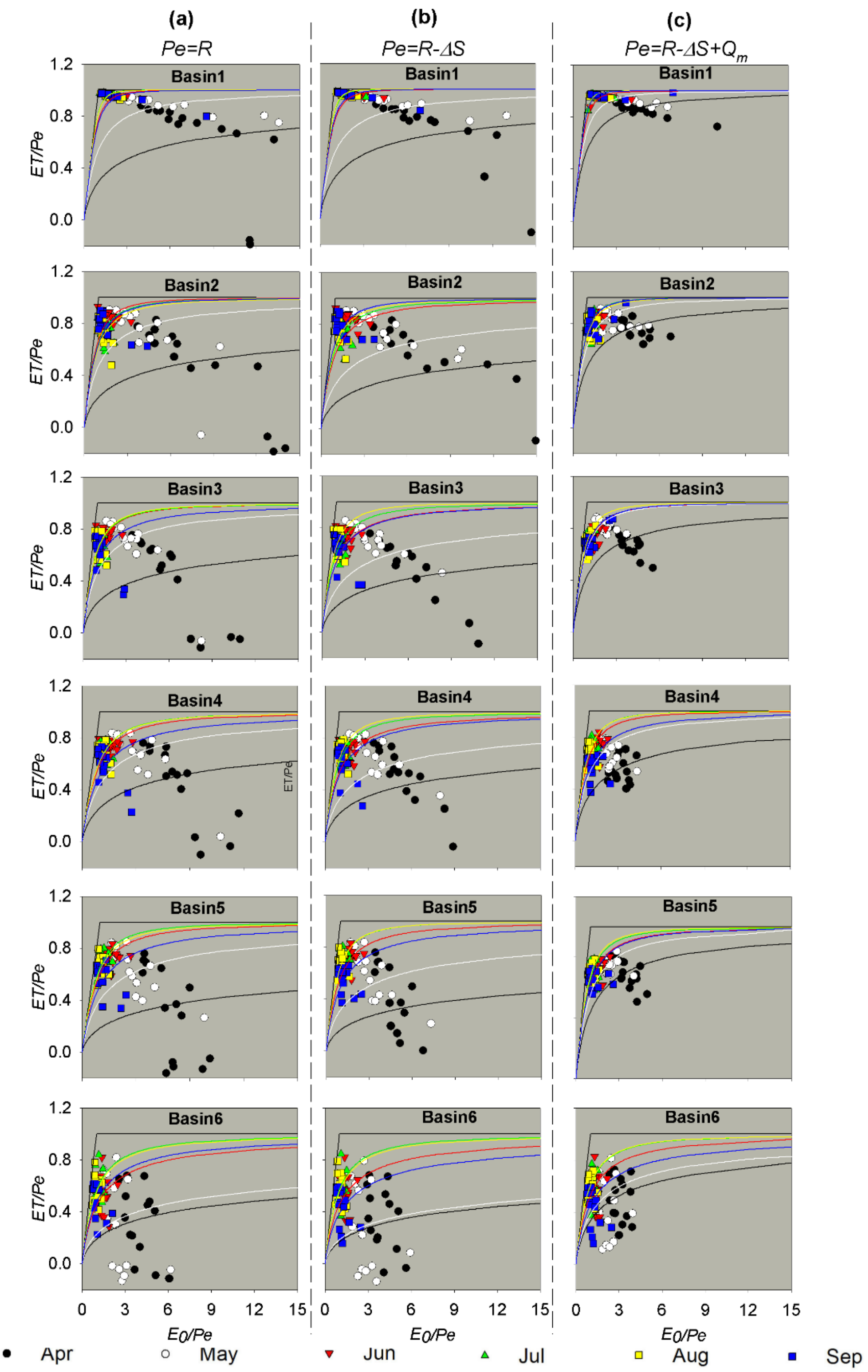

Figure 3 Plots for the aridity index vs. evapotranspiration index scaled by the available water supply for monthly series in the growing season. The total water availability is (a) R, (b) $R-\Delta S$, (c) $R+Q_m-\Delta S$. The n value for each Budyko curve is fitted by long-term averaged monthly data.

4.2 Variations in the growing season water balance

The mean and standard deviation (σ) for each item in the growing season water balance in the six basins are summarised in Tables 1 and 2. The proportion of ΔS in the water balance was small, with a mean value of 1.2 mm; however, its intra-annual fluctuation was relatively large, with a $\sigma_{\Delta S}$ of 5.3 mm, and $\sigma_{\Delta S}$ was even as high as 9.0 mm in Basin 6. Compared to ΔS, Q_m represented a larger proportion of the water balance with a mean of 8.5±6.5 mm, indicating its important role in the basin water supply. For this region, the water supply of ET was not only R but also included Q_m and ΔS. Consequently, the mean monthly ET generally approached R (55.8±27.4 mm) or higher values in Basin 1.

Table 1 Averaged monthly hydrometeorological characteristics and vegetation coverage in the growing season (2001–2014).

ID	Station	Area	R	Q_m	ΔS	E_0	M	n	E
1	Dangchengwan	14325	57.2	8.6	0.7	126.7	0.08	3.08	59.1
2	Changmabu	10961	68.9	10.8	1.1	123.0	0.13	1.79	59.3
3	Zhamashike	4986	73.5	10.6	1.5	120.3	0.40	1.59	59.1
4	Qilian	2452	74.5	9.0	1.4	116.8	0.44	1.37	54.9
5	Yingluoxia	10009	77.2	7.4	1.1	117.4	0.53	1.35	55.1
6	Shagousi	1600	83.5	4.8	1.4	116.3	0.48	1.01	47.1

The change patterns of the monthly R, ΔS, Q_m, and ET during the growing season are presented in Figure 4 and Supplementary Figures S1–S3. R exhibited a regular unimodal trend, with a maximum value occurring in July. The maximum Q_m appeared in May, which is a result that is in agreement with previous studies in this region (Wang and Qin, 2017; Zhang et al., 2016c). The peak of ΔS lagged that of Q_m for one month in Basins 1–4 and three months in Basins 5–6, indicating a recharge of soil water by snowmelt. Yang et al. (2015) also detected the time differences between ΔS and Q_m and found that ΔS had a time lag of 3–4 months more than did Q_m in the Tarim River Basin, another arid alpine basin in north-western China with hydroclimatic conditions similar to those of the study region. Further, the abundant R in July should contribute to more available water for ΔS; however, the ΔS in July was relatively small. This can be partially explained by the higher water consumption, i.e. the ET in July. In a manner similar to the change pattern of R, ET exhibited a unimodal trend, suggesting the crucial role of R.

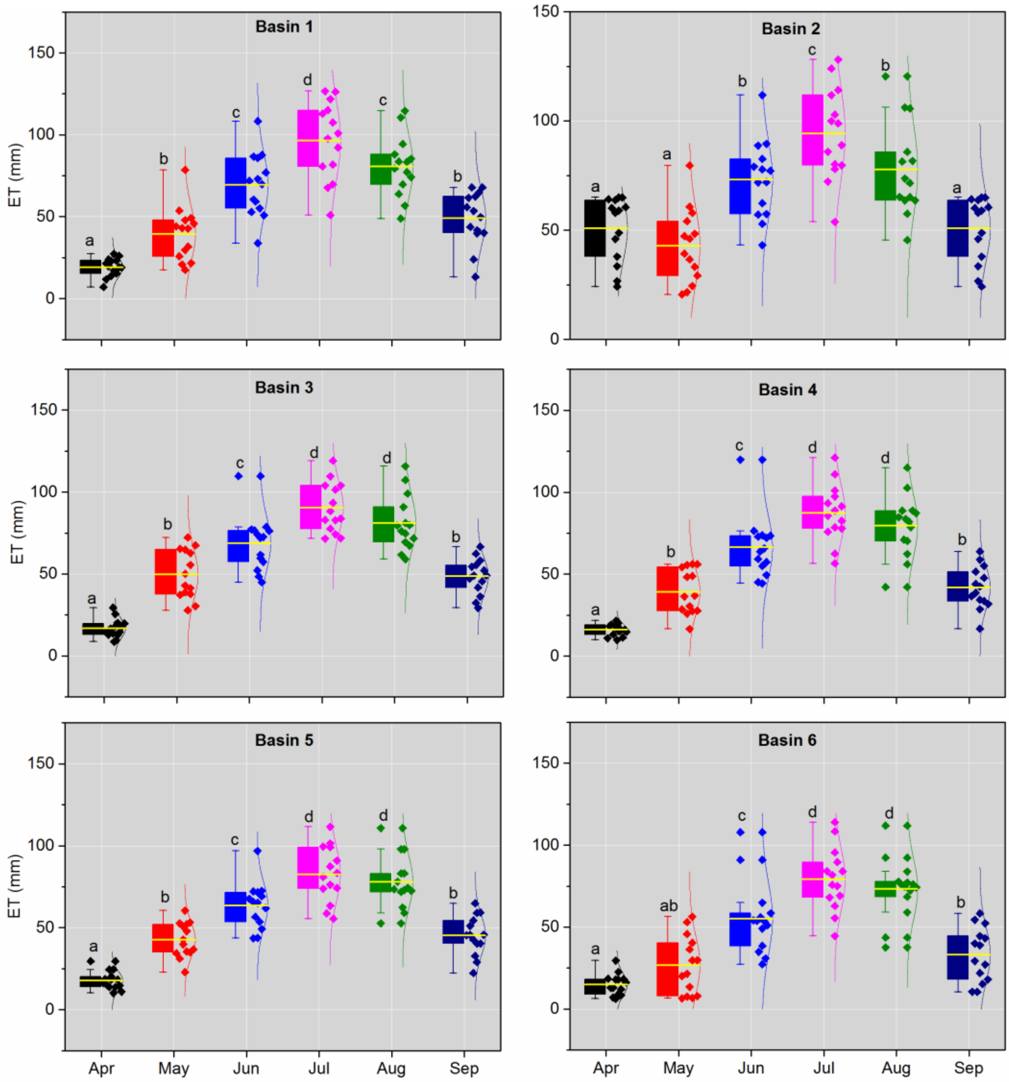

Figure 4 Variations in the monthly *ET* for each basin during 2001–2014. A distribution curve is shown to the right side of each box plot, and the data points are represented by diamonds. Different letters indicate significant differences at $p < 0.05$.

4.3 Controlling factors of the *ET* variance

The contributions of R, E_0, Q_m, ΔS, and M to σ_{ET}^2 for each basin are shown in Figure 5. The results showed that the variance of these five factors could explain σ_{ET}^2, with the total contribution rates ranging from 56.5% (Basin 6) to 98.6% (Basin 1). With the decreasing ϕ from Basin 1 to Basin 6, C(R) showed an increasing trend, ranging from 40.6% to 94.2%; conversely, C(E_0) exhibited a decreasing trend, ranging from 0.2% to 4.1%. This result indicated that R played a key role in σ_{ET}^2 in this region. Similarly, Zhang et al. (2016a) found that C(P) increased rapidly with increasing ϕ, whereas C(E_0) decreased rapidly based on 282 basins in China. Our results are also consistent with previous conclusions that changes in ET or Q_r are dominated by changes in water conditions rather than by energy conditions in dry regions (Berghuijs et al., 2017; Yang et al., 2006; Zeng and Cai, 2016; Zhang et al., 2016a).

The M variance had the second largest contribution to σ_{ET}^2 with a mean C(M) value of 4.3% for the six basins. Specifically, C(M) showed an increasing trend from 0.5% to 9.5% with the decreasing ϕ, implying that the contribution of vegetation change to ET variance was larger in relatively humid basin. It can be explained that transpiration is more sensitive to vegetation change, and thus the higher vegetation coverage could increase the proportion of transpiration to ET in humid regions (Niu et al., 2019; Zhang et al., 2020). The Budyko hypothesis stated that change in ET is controlled by change in available energy when water supply is not a limiting factor under humid conditions (Budyko, 1974; Yang et al., 2006). The increasing M results in the reallocation of available energy between canopy and soil. Specifically, more energy is consumed by canopy thus increases transpiration. Further, Previous studies have found that ET differs greatly among species, because of the difference in canopy roughness, the timing of physiological functioning, water holding capacity of the soil and rooting depth of the vegetation (Baldocchi et al., 2004; Bruemmer et al., 2012). Generally, forest had larger ET than grassland (Ma et al., 2020; Zha et al., 2010). The fraction of forest area is relatively high and thus lead to the higher contributions to ET for whole basin in the humid region. For example, Wei et al. (2018) showed that the global average variation in the annual Q_r due to the vegetation cover change was 30.7±22.5% in forest-dominated regions on long-term scales, which was higher than our results because of their higher forest cover.

The contribution of the Q_m variance ranked third with a mean value of 1.8%. Similar as C(R), C(Q_m) showed a downward trend with the decreasing ϕ, ranging from 2.9% to 0.4%. The larger C(Q_m) can be explained by the larger variance in Q_m in Basins 2–4 (σ values in Table 2). However, the Q_m in Basin 1 was only 8.6 mm, and C(Q_m) was the largest in all six sub-basins (2.9%). It can be explained that the contribution of each variable to σ_{ET}^2 was not only the product of the partial differential coefficients, but also relied on its variance value according to Equation 14. Specifically, the partial differential coefficients of 0.1 for a variable means that a 10% change in that variable may result in a change in ET by 1%, which can only reflect the theoretical contribution of each variable. By multiplying the variance value, the actual contribution of each variable could be obtained. The ε_{Q_m} value was the largest in Basin 1 and thus led to the largest C(Q_m). In addition, shifts in the snowmelt period can also partially explain the positive contribution of the Q_m variance. Like many snow-dominated regions of the world (Barnett et al., 2005), climate warming shifted the timing of snowmelt earlier in the spring in the Qilian Mountains (Li et al., 2012). Earlier snowmelt due to a warmer atmosphere resulted in increased soil moisture and a greater proportion of Q_m to ET (Barnhart et al., 2016; Bosson et al., 2012).

Previous studies have considered that most precipitation changes are transferred to water storage (Wang and Hejazi, 2011); thus, ΔS has distinct impacts on the intra-annual ET or Q_r variance in arid regions (Ye et al., 2015; Zeng and Cai, 2016; Zhang et al., 2016a). However, the study region under investigation has a small C(ΔS) with a mean value of 1.02%, which is likely to be caused by the vegetation conditions and time-scale. First, the six basins have higher vegetation coverage compared to other arid basins; consequently, plant transpiration and rainfall interception consume most of the water supply and reduce the transformation of rainfall to water storage. This is consistent with previous studies that showed that the fractional contribution of transpiration to ET would increase with increasing woody cover (Villegas et al., 2010; Wang et al., 2010b). Second, the large contribution of ΔS to the intra-annual ET or Q_r variance in arid regions is mostly detected at monthly scales. The smaller ΔS in the non-growing season will increase the annual value of $\sigma_{\Delta S}$. However, this study focused on the growing season with a smaller $\sigma_{\Delta S}$, which consequently led to a lower C(ΔS).

4.4 Interaction effects between controlling factors on the *ET* variance

The interaction effect of two factors on the *ET* variance was represented by their covariance coefficients using Equations 15 and 16 (Figure 5). Among the ten groups of interaction effects, the coupled *R* and *M* had the largest contribution to the *ET* variance, with a mean value of 24.3%. The positive covariance of *R* and *M* indicated that *M* changes in-phase with *R* (i.e. *R* occurred in the growing season), thus increasing the *ET* variance. C(*R_M*) showed an increasing trend from 9.9% to 34.6% with decreasing ϕ. With different water conditions, the types and proportions of the main ecosystems varied across basins. In particular, *F* showed an increasing trend with decreasing ϕ, which partially explained the spatial variations in C(*R_M*). Previous studies concluded that the differences in physiological and phenological characteristics of ecosystem types are likely to modulate the response of the ecosystem *ET* to climate variability (Bruemmer et al., 2012; Falge et al., 2002; Li et al., 2019a). For example, Yuan et al. (2010) found that, at the beginning of the growing season, a significantly higher *ET* was observed in evergreen needleleaf forests; however, during the middle term of the growing season (June–August), the *ET* was largest in deciduous broadleaf forests in a typical Alaskan basin.

As an indicator of climate seasonality, the covariance of *R* and E_0 indicates matching conditions between the water and energy supplies, such as the phase difference between the storm season and warm season. A positive cov(R, E_0) suggests an in-phase R change with E_0 and consequently increases the ET variance. In this study, following C(R_M), the coupled R and E_0 had a large impact on the ET variance with a mean contribution of 14.1%. With a typical temperate continental climate, the study area has in-phase water and energy conditions; however, its ET is limited by the water supply in spite of the abundant energy supply (Yang et al., 2006). The vegetation receives the largest water supply in the growing season and can vary its biomass seasonally in order to adapt to the R seasonality (Potter et al., 2005; Ye et al., 2016). Consequently, the impact of climate variability on ET variance was mainly reflected by the R seasonality in the study area.

In comparison, the interacting effects between R and Q_m, M and Q_m, R and ΔS, and Q_m and E_0 contributed negatively to the ET variance. Among them, the effect of the coupled R and Q_m was largest with a C(R_Q_m) of −7.6%. This may suggest that Q_m changes were out-of-phase with R. Specifically, the major snow melting period was from March to May, when snowmelt water accounts for ~70% of the water supply; however, ~ 65% of the annual R occurred in the summer (June–August) (Li et al., 2019a). Overall, Q_m sustains the ET in the spring, but R supports the ET in the summer.

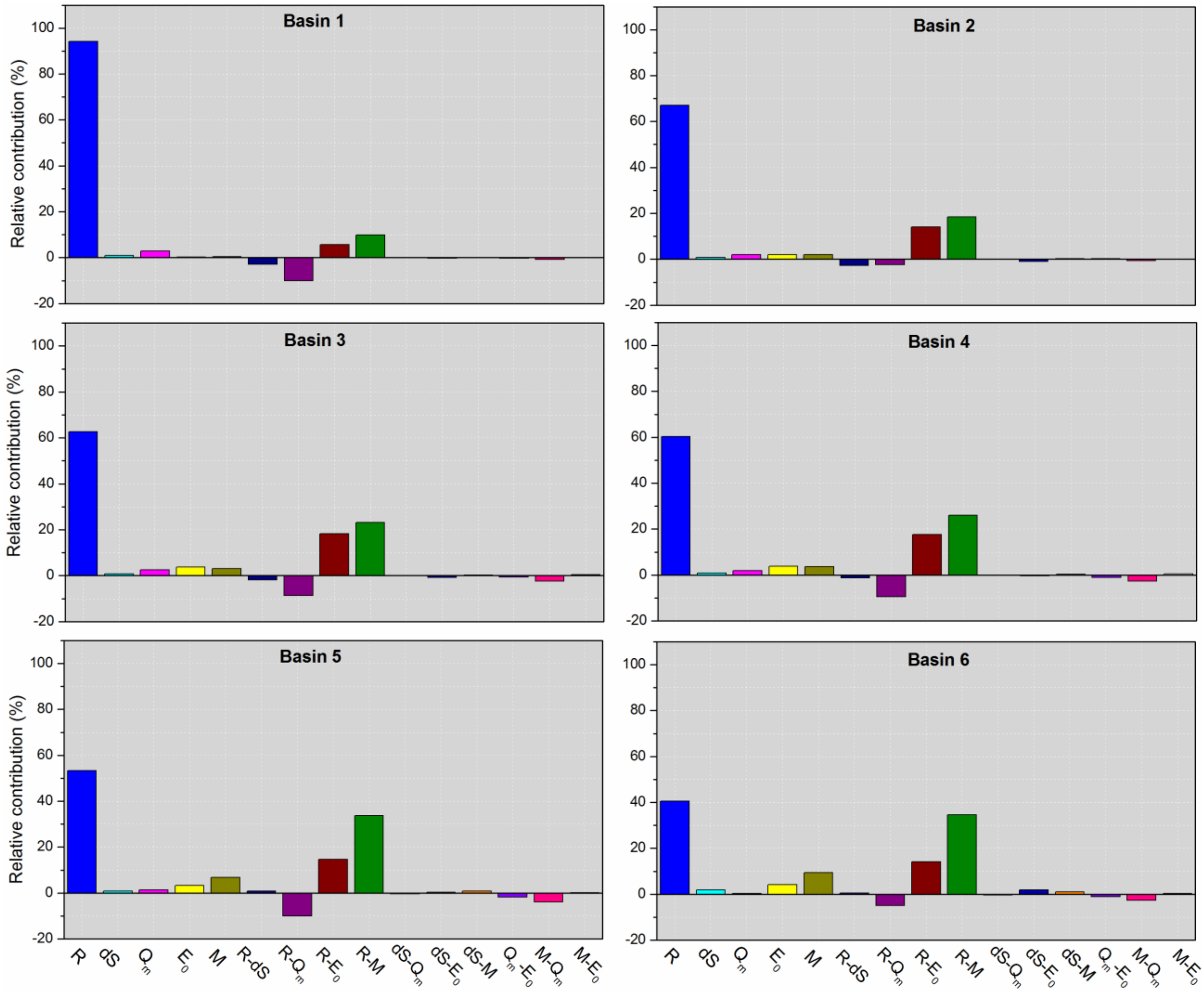

Figure 5 Contribution to the *ET* variance in the growing season from each component in Equation 15.

4.5 Uncertainties

Uncertainties from different sources may result in errors for this study. First, this study estimated ΔS and Q_m with the GLDAS Noah land surface model and the degree-day model, respectively. Although the GLDAS_ΔS has been widely used in hydrological studies, it ignores the change in deep groundwater (Nie et al., 2016; Syed et al., 2008;

Zhang et al., 2016), which may lead to errors in ET estimation based on water balance equation. But previous studies showed that the groundwater change in our study area is relatively small, and can thus be ignored. For example, Du et al. (2016) used the abcd model to quantitatively determine monthly variations of water balance for the sub-basins of Heihe River (including basins 3-5 in our study) and found that the soil water storage change have obvious effects on the monthly water balance, whilst the impact of monthly groundwater storage change is negligible. Furthermore, it has been found that any change in climate conditions and underlying basin characteristics will affect the contributions of heat balance components and cause temporal variations of DDF (Kuusisto, 1980; Ohmura, 2001). But previous studies indicated that there is no significant seasonal change in DDF in west China (Zhang et al., 2006); as such, it is acceptable to estimate snowmelt runoff using fixed DDF values in this study. In comparison, the contribution of snow meltwater to runoff (F_s) was 12.9% in Basin 2 during 1971-2015 by using Spatial Processes in Hydrology model(Li et al., 2019), while F_s was 25% in Basin 3 from 2001 to 2012 based on geomorphology-based ecohydrological model (Li et al., 2018), <10% in Basin 6 during 1961-2006 by using SRM model (Gao et al., 2011). Our results indicated that the F_s in Basin 2, 3 and 6 were 14.8%, 24.5% and 6.7%, respectively, which were close to those from different models. Finally, the uncertainties of ΔS and Q_m may lead to errors in ET estimation by water balance equation. To validate the reliability of our estimated ET, the comparison with ET_{map} from May to September during 2012-2014 was conducted (Figure S4). The results showed that our estimated ET fitted well with ET_{map} and basically fell around the 1:1 line, indicating ET estimated using water balance equation by considering the items of ΔS and Q_m is acceptable. However, it cannot be ignored that our estimated ET was generally lower than ET_{map}. The error of rainfall spatial interpolation may explain the underestimation of ET. Most meteorological stations are located at low elevations or in river valleys, but some stations are distributed in high elevations in Qilian Mountain (Figure 1). It has been found that rainfall in mountainous regions is generally larger than that in plain regions (Qiang et al., 2015). Even the topography effect was considered for interpolation, it still resulted in bias in areal rainfall. The best method to improve the quality of spatial rainfall estimation is to increase the density of the monitoring network. However, this process is limited by harsh environment and funds (Buytaert et al., 2006). The errror of rainfall will be transferred to contribution quantification of ET variance by underestimating rainfall contribution, while overestimating Q_m and ΔS contribution.

Second, previous studies concluded that three main factors could be responsible for the variability of n, including underlying physical conditions (such as soil and topography characteristics) (Milly, 1994; Yang et al., 2009), climate seasonality (such as the temporal variability of rainfall, mismatch between water and energy) (Ning et al., 2017; Potter et al., 2005) and vegetation dynamics (Donohue et al., 2007; Zhang et al., 2001). On the short time scale, the changes in soil and topography are negligible and its impact on the variability of n can be ignored. In consequence, the factors, should be considered, are climate seasonality and vegetation dynamics. When parameterizing n, this study considered M but ignored climate seasonality since the covariance item between R and E_0, i.e. $\varepsilon_1\varepsilon_4\mathrm{cov}(R, E_0)$ in the Equation (15) can represent climate seasonality. In addition, human influence represented by parameter n on the water balance cannot be ignored, which remains further investigation.

5 Conclusion

Recently, several studies have applied a variance decomposition framework based on the Budyko equation to elucidate the dominant driving factors of the ET variance at annual and intra-annual scales by decomposing the intra-annual ET variance into the variance/covariance of P, E_0, and ΔS. Vegetation changes can greatly affect the ET variability, but their effects on the ET variance on finer time-scales was not quantified by this decomposed method. Further, in snow-dependent regions, snowpack stores precipitation in winter and releases water in spring; thus, Q_m plays an important role in the hydrological cycle. Therefore, it is also necessary to consider the role of the Q_m changes on the ET variability.

In this study, six arid alpine basins in the Qilian Mountains of northwest China were chosen as examples. The monthly Q_m during 2001–2014 was estimated using the degree-day model, and the growing season ET was calculated using the water balance equation ($ET = R + Q_s - Q_r - \Delta S$). The controlling parameter n of the Choudhury–Yang equation was found to be closely correlated with M, as estimated by *NDVI* data. Thus, by combining the Choudhury–Yang equation with the semi-empirical formula between n and M, the growing season σ_{ET}^2 is decomposed into the temporal variance and covariance of R, E_0, ΔS, Q_m, and M. The main results showed that considering Q_m and ΔS in the water balance equation can improve the performance of the Budyko framework in snow-dependent basins on a monthly scale; σ_{ET}^2 was primarily enhanced by the R variance, followed by the coupled R and M and then the coupled R and E_0. The enhancing effects of the variance in M and Q_m cannot be ignored; however, the interactions between R and Q_m, M and Q_m, R and ΔS, and Q_m and E_0 dampened σ_{ET}^2. As a simple and effective method, our extended *ET* variance decomposition method has the potential to be widely used to assess the hydrological responses to changes in the climate and vegetation in snow-dependent regions at finer time-scales.

Table 2 The elasticity coefficients of ET for five variables and the standard deviation of each variable for the six basins.

Basin	Elasticity coefficients					Standard deviation						
	ε_R	ε_{Q_m}	$\varepsilon_{\Delta S}$	ε_{E_0}	ε_M	σ_R, mm	σ_{Q_m}, mm	$\sigma_{\Delta S}$, mm	σ_{E_0}, mm	σ_M	Predicted σ_{ET}, mm	Assessed σ_{ET}, mm
1	0.85	0.85	−0.85	0.06	41.94	34.4	6.0	3.4	25.5	0.05	30.2	31.2
2	0.56	0.56	−0.56	0.16	55.84	40.6	7.0	4.3	24.7	0.07	27.8	30.3
3	0.46	0.46	−0.46	0.20	20.81	42.5	8.5	4.9	23.6	0.21	24.9	27.9
4	0.44	0.44	−0.44	0.19	20.58	40.1	7.2	4.8	23.1	0.21	22.5	25.8
5	0.43	0.43	−0.43	0.19	24.60	39.8	6.3	5.1	22.0	0.25	23.3	25.0
6	0.33	0.33	−0.33	0.18	31.51	41.2	4.0	9.0	23.6	0.21	21.3	24.3

Data availability

The Digital elevation data are available at http://www.gscloud.cn/sources/accessdata/310?pid=302. Meteorological data are available at http://data.cma.cn/data/detail/dataCode/SURF_CLI_CHN_MUL_DAY_CES_V3.0.html. The runoff records were obtained from the Bureau of Hydrology and Water Resources, Gansu Province. The GLDAS data are available at https://disc.gsfc.nasa.gov/datasets/GLDAS_NOAH025_M_2.0/summary. MODIS MOD10A2 Version 6 snow cover products are available at https://nsidc.org/data/mod10a2. MODIS MOD13A3.006 products are available at https://lpdaac.usgs.gov/products/mod13a3v006/. The dataset of "ground truth of land surface evapotranspiration at regional scale in the Heihe River Basin (2012-2016) ETmap Version 1.0" are available at http://data.tpdc.ac.cn/zh-hans/data/8efbb18d-bc02-4bf6-9f21-345480d6637f/?q=ETMap.

Author contributions

Tingting Ning: Methodology, Writing–original draft, Software, Visualisation

Zhi Li: Writing–review & editing

Qi Feng: Conceptualisation, Supervision

Zongxing Li and Yanyan Qin: Data curation, Resources

Competing interests

The authors declare that they have no conflicts of interest.

Acknowledgements

This study was supported by the National Natural Science Foundation of China (41807160), Opening Research Foundation of Key Laboratory of Land Surface Process and Climate Change in Cold and Arid Regions, Chinese Academy of Sciences (LPCC 2020003), the "Western Light"-Key Laboratory Cooperative Research Cross-Team Project of Chinese Academy of Sciences, the CAS 'Light of West China' Program (Y929651001), the Major Program of the Natural Science Foundation of Gansu Province, China (18JR4RA002) , and the Second Tibetan Plateau Scientific Expedition and Research Program (STEP, Grant No.2019QZKK0405).

References

Baldocchi, D.D., Xu, L.K. and Kiang, N., 2004. How plant functional-type, weather, seasonal drought, and soil physical properties alter water and energy fluxes of an oak-grass savanna and an annual grassland. *Agricultural and Forest Meteorology*, 123(1-2): 13-39.

Barnett, T.P., Adam, J.C. and Lettenmaier, D.P., 2005. Potential impacts of a warming climate on water availability in snow-dominated regions. *Nature*, 438(7066): 303-309.

Barnhart, T.B., Molotch, N.P., Livneh, B., Harpold, A.A., Knowles, J.F. and Schneider, D., 2016. Snowmelt rate dictates streamflow. *Geophysical Research Letters*, 43(15): 8006-8016.

Berghuijs, W.R., Larsen, J.R., Van Emmerik, T.H.M. and Woods, R.A., 2017. A Global Assessment of Runoff Sensitivity to Changes in Precipitation, Potential Evaporation, and Other Factors. *Water Resources Research*, 53: 8475-8486.

Bosson, E., Sabel, U., Gustafsson, L.-G., Sassner, M. and Destouni, G., 2012. Influences of shifts in climate, landscape, and permafrost on terrestrial hydrology. *Journal of Geophysical Research-Atmospheres*, 117: D05120.

Bourque, C.P.A. and Mir, M.A., 2012. Seasonal snow cover in the Qilian Mountains of Northwest China: Its dependence on oasis seasonal evolution and lowland production of water vapour. *Journal of Hydrology*, 454: 141-151.

Bruemmer, C., Black, T.A., Jassal, R.S., Grant, N.J., Spittlehouse, D.L., Chen, B., Nesic, Z., Amiro, B.D., Arain, M.A., Barr, A.G., Bourque, C.P.A., Coursolle, C., Dunn, A.L., Flanagan, L.B., Humphreys, E.R., Lafleur, P.M., Margolis, H.A., McCaughey, J.H. and Wofsy, S.C., 2012. How climate and vegetation type influence evapotranspiration and water use efficiency in Canadian forest, peatland and grassland ecosystems. *Agricultural and Forest Meteorology*, 153: 14-30.

Budyko, M.I., 1961. Determination of evaporation from the land surface (in Russian). *Izvestiya Akad.nauk Sssr.ser.geograf.geofiz*, 6: 3-17.

Budyko, M.I., 1974. Climate and life. Academic, New York.

Buytaert, W., Celleri, R., Willems, P., Bièvre, B.D. and Wyseure, G., 2006. Spatial and temporal rainfall variability in mountainous areas: A case study from the south Ecuadorian Andes. *Journal of Hydrology*, 329(3-4): 413-421.

Chen, X., Alimohammadi, N. and Wang, D., 2013. Modeling interannual variability of seasonal evaporation and storage change based on the extended Budyko framework. *Water Resources Research*, 49(9): 6067-6078.

Choudhury, B.J., 1999. Evaluation of an empirical equation for annual evaporation using field observations and results from a biophysical model. *Journal of Hydrology*, 216(1-2): 99-110.

Cong, Z., Shahid, M., Zhang, D., Lei, H. and Yang, D., 2017. Attribution of runoff change in the alpine basin: a case study of the Heihe Upstream Basin, China. *Hydrological Sciences Journal-Journal Des Sciences Hydrologiques*, 62(6):

1013-1028.

Deng, S., Yang, T., Zeng, B., Zhu, X. and Xu, H., 2013. Vegetation cover variation in the Qilian Mountains and its response to climate change in 2000-2011. *Journal of Mountain Science*, 10(6): 1050-1062.

Donohue, R.J., Roderick, M.L. and McVicar, T.R., 2007. On the importance of including vegetation dynamics in Budyko's hydrological model. *Hydrology and Earth System Sciences,* 11(2): 983-995.

Du, C., Sun, F., Yu, J., Liu, X. and Chen, Y., 2016. New interpretation of the role of water balance in an extended Budyko hypothesis in arid regions. *Hydrology and Earth System Sciences*, 20(1): 393-409.

Du, J., He, Z., Piatek, K.B., Chen, L., Lin, P. and Zhu, X., 2019. Interacting effects of temperature and precipitation on climatic sensitivity of spring vegetation green-up in arid mountains of China. *Agricultural and Forest Meteorology*, 269: 71-77.

Falge, E., Baldocchi, D., Tenhunen, J., Aubinet, M., Bakwin, P., Berbigier, P., Bernhofer, C., Burba, G., Clement, R., Davis, K.J., Elbers, J.A., Goldstein, A.H., Grelle, A., Granier, A., Guomundsson, J., Hollinger, D., Kowalski, A.S., Katul, G., Law, B.E., Malhi, Y., Meyers, T., Monson, R.K., Munger, J.W., Oechel, W., Paw, K.T., Pilegaard, K., Rannik, U., Rebmann, C., Suyker, A., Valentini, R., Wilson, K.

and Wofsy, S., 2002. Seasonality of ecosystem respiration and gross primary production as derived from FLUXNET measurements. *Agricultural and Forest Meteorology*, 113(1-4): 53-74.

Feng, S., Liu, J., Zhang, Q., Zhang, Y., Singh, V.P., Gu, X. and Sun, P., 2020. A global quantitation of factors affecting evapotranspiration variability. *Journal of Hydrology*, 584: 124688 .

Feng, X., Fu, B., Piao, S., Wang, S. and Ciais, P., 2016. Revegetation in China's Loess Plateau is approaching sustainable water resource limits. *Nature Climate Change*, 6: 1019-1022.

Gao, X., Zhang, S., Ye, B. and Gao, H., 2011. Recent changes of glacier runoff in the Hexi Inland river basin. *Advances in Water Science (In Chinese)*, 22(3): 344-350.

Godsey, S.E., Kirchner, J.W. and Tague, C.L., 2014. Effects of changes in winter snowpacks on summer low flows: case studies in the Sierra Nevada, California, USA. *Hydrological Processes*, 28(19): 5048-5064.

Griessinger, N., Seibert, J., Magnusson, J. and Jonas, T., 2016. Assessing the benefit of snow data assimilation for runoff modeling in Alpine catchments. *Hydrology and Earth System Sciences*, 20(9): 3895-3905.

Hock, R., 2003. Temperature index melt modelling in mountain areas. *Journal of Hydrology*, 282(1-4): 104-115.

Huning, L.S. and AghaKouchak, A., 2018. Mountain snowpack response to different levels of warming. *Proceedings of the National Academy of Sciences of the United States of America*, 115(43): 10932-10937.

Katul, G.G., Oren, R., Manzoni, S., Higgins, C. and Parlange, M.B., 2012. Evapotranspiration: a process driving mass transport and energy exchange in the soil-plant-atmosphere-cliamte system. *Reviews of Geophysics*, 50: RG3002.

Koster, R.D. and Suarez, M.J., 1999. A simple framework for examining the interannual variability of land surface moisture fluxes. *Journal of Climate*, 12(7): 1911-1917.

Kuusisto, E., 1980. On the values and variability of degree-day melting factor in Finland. *Nordic Hydrology*, 11(5): 235-242.

Lan, Y., Hu, X., Din, H., La, C. and Song, J., 2012. Variation of Water Cycle Factors in the Western Qilian Mountain Area under Climate WarmingTaking the Mountain Watershed of the Main Stream of Shule River Basin for Example. *Journal of Mountain Science （in Chinese）*, 30(6): 675-680.

Li, B., Chen, Y., Chen, Z. and Li, W., 2012. The Effect of Climate Change during

Snowmelt Period on Streamflow in the Mountainous Areas of Northwest China. *Acta Geographica Sinica (In Chinese*）, 67(11): 1461-1470.

Li, D., Pan, M., Cong, Z., Zhang, L. and Wood, E., 2013. Vegetation control on water and energy balance within the Budyko framework. *Water Resources Research*, 49(2): 969-976.

Li, H., Zhao, Q., Wu, J., Ding, Y., Qin, J., Wei, H. and Zeng, D., 2019. Quantitative simulation of the runoff components and its variation characteristics in the upstream of the Shule River. *Journal of Glaciology and Geocryology (in Chinese)*, 41(4): 907-917.

Li, L.L., Li, J., Chen, H.M. and Yu, R.C., 2019a. Diurnal Variations of Summer Precipitation over the Qilian Mountains in Northwest China. *Journal of Meteorological Research*, 33(1): 18-30.

Li, S., Zhang, L., Kang, S., Tong, L., Du, T., Hao, X. and Zhao, P., 2015. Comparison of several surface resistance models for estimating crop evapotranspiration over the entire growing season in arid regions. *Agricultural and Forest Meteorology*, 208: 1-15.

Li, X., Cheng, G., Ge, Y., Li, H., Han, F., Hu, X., Tian, W., Tian, Y., Pan, X., Nian, Y., Zhang, Y., Ran, Y., Zheng, Y., Gao, B., Yang, D., Zheng, C., Wang, X., Liu, S. and Cai, X., 2018. Hydrological Cycle in the Heihe River Basin and Its

Implication for Water Resource Management in Endorheic Basins. *Journal of Geophysical Research-Atmospheres*, 123(2): 890-914.

Li, Z., Feng, Q., Li, Z., Yuan, R., Gui, J. and Lv, Y., 2019b. Climate background, fact and hydrological effect of multiphase water transformation in cold regions of the Western China: A review. *Earth-Science Reviews*, 190: 33-57.

Li, Z., Feng, Q., Wang, Q.J., Yong, S., Cheng, A. and Li, J., 2016. Contribution from frozen soil meltwater to runoff in an in-land river basin under water scarcity by isotopic tracing in northwestern China. *Global and Planetary Change*, 136: 41-51.

Liu, J., Zhang, Q., Feng, S., Gu, X., Singh, V.P. and Sun, P., 2019. Global Attribution of Runoff Variance Across Multiple Timescales. *Journal of Geophysical Research-Atmospheres*, 124(24): 13962-13974.

Liu, J., Zhang, Q., Singh, V.P., Song, C., Zhang, Y. and Sun, P., 2018. Hydrological effects of climate variability and vegetation dynamics on annual fluvial water balance at global large river basins. *Hydrology & Earth System Sciences*, 22: 4047-4060.

Ma, S., Eichelmann, E., Wolf, S., Rey-Sanchez, C. and Baldocchi, D.D., 2020. Transpiration and evaporation in a Californian oak-grass savanna: Field measurements and partitioning model results. *Agricultural and Forest*

Meteorology, 295: 108204.

Ma, Z., Kang, S., Zhang, L., Tong, L. and Su, X., 2008. Analysis of impacts of climate variability and human activity on streamflow for a river basin in arid region of northwest China. *Journal of Hydrology*, 352(3-4): 239-249.

Matin, M.A. and Bourque, C.P.A., 2015. Mountain-river runoff components and their role in the seasonal development of desert-oases in northwest China. *Journal of Arid Environments*, 122: 1-15.

Maurya, A.S., Rai, S.P., Joshi, N., Dutt, K.S. and Rai, N., 2018. Snowmelt runoff and groundwater discharge in Himalayan rivers: a case study of the Satluj River, NW India. *Environmental Earth Sciences*, 77(19): 694.

Milly, P.C.D, 1994. Climate,soil-water storage, and the average annual water-balance. W*ater Resources Research*, 30(7): 2143-2156.

Nie, N., Zhang, W.C., Zhang, Z.J., Guo, H.D. and Ishwaran, N., 2016. Reconstructed Terrestrial Water Storage Change (Delta TWS) from 1948 to 2012 over the Amazon Basin with the Latest GRACE and GLDAS Products. *Water Resources Management*, 30(1): 279-294.

Ning, T., Li, Z. and Liu, W. , 2017. Vegetation dynamics and climate seasonality jointly control the interannual catchment water balance in the Loess Plateau under the

Budyko framework. *Hydrology and Earth System Sciences*, 21(3): 1515-1526.

Ning, T., Li, Z., Feng, Q., Chen, W. and Li, Z., 2020. Effects of forest cover change on catchment evapotranspiration variation in China. *Hydrological Processes*, 34(10): 2219-2228.

Niu, Z., He, H., Zhu, G., Ren, X., Zhang, L., Zhang, K., Yu, G., Ge, R., Li, P., Zeng, N. and Zhu, X., 2019. An increasing trend in the ratio of transpiration to total terrestrial evapotranspiration in China from 1982 to 2015 caused by greening and warming. *Agricultural and Forest Meteorology*, 279: 107701 .

Ohmura, A., 2001. Physical basis for the temperature-based melt-index method. *Journal of Applied Meteorology*, 40(4): 753-761.

Potter, N.J., Zhang, L., Milly, P.C.D., McMahon, T.A. and Jakeman, A.J., 2005. Effects of rainfall seasonality and soil moisture capacity on mean annual water balance for Australian catchments. *Water Resources Research*, 41(6): W06007.

Priestley, C. and Taylor, R., 1972. On the assessment of surface heat flux and evaporation using large-scale parameters. *Monthly Weather Review*, 100(2): 81-92.

Qiang, F., Zhang, M.J., Wang, S., Liu, Y., Ren, Z. and Zhu, X., 2015. Changes of areal precipitation based on gridded dataset in Qilian Mountains during 1961-2012.

Acta Geographica Sinica (In Chinese), 70(7): 1125-1136.

Qin, Y., Abatzoglou, J.T., Siebert, S., Huning, L.S., AghaKouchak, A., Mankin, J.S., Hong, C., Tong, D., Davis, S.J. and Mueller, N.D., 2020. Agricultural risks from changing snowmelt. *Nature Climate Change*, 10(5): 459-465.

Ragettli, S., Pellicciotti, F., Immerzeel, W.W., Miles, E.S., Petersen, L., Heynen, M., Shea, J.M., Stumm, D., Joshi, S. and Shrestha, A., 2015. Unraveling the hydrology of a Himalayan catchment through integration of high resolution in situ data and remote sensing with an advanced simulation model. *Advances in Water Resources*, 78: 94-111.

Rice, R., Bales, R.C., Painter, T.H. and Dozier, J., 2011. Snow water equivalent along elevation gradients in the Merced and Tuolumne River basins of the Sierra Nevada. *Water Resources Research*, 47: W08515.

Rodriguez-Iturbe, I., 2000. Ecohydrology: A hydrologic perspective of climate-soil-vegetation dynamics. *Water Resources Research*, 36(1): 3-9.

Semadeni-Davies, A., 1997. Monthly snowmelt modelling for large-scale climate change studies using the degree day approach. *Ecological Modelling*, 101(2-3): 303-323.

Stewart, I.T., 2009. Changes in snowpack and snowmelt runoff for key mountain regions. *Hydrological Processes*, 23(1): 78-94.

Stewart, I.T., Cayan, D.R. and Dettinger, M.D., 2005. Changes toward earlier streamflow timing across western North America. *Journal of Climate*, 18(8): 1136-1155.

Syed, T.H., Famiglietti, J.S., Rodell, M., Chen, J. and Wilson, C.R., 2008. Analysis of terrestrial water storage changes from GRACE and GLDAS. *Water Resources Research*, 44(2): W02433.

Villegas, J.C., Breshears, D.D., Zou, C.B. and Law, D.J., 2010. Ecohydrological controls of soil evaporation in deciduous drylands: How the hierarchical effects of litter, patch and vegetation mosaic cover interact with phenology and season. *Journal of Arid Environments*, 74(5): 595-602.

Wagle, P. and Kakani, V.G., 2014. Growing season variability in evapotranspiration, ecosystem water use efficiency, and energy partitioning in switchgrass. *Ecohydrology*, 7(1): 64-72.

Wang, D. and Hejazi, M., 2011. Quantifying the relative contribution of the climate and direct human impacts on mean annual streamflow in the contiguous United States. *Water Resources Research*, 47: W00J12.

Wang, J., Li, H. and Hao, X., 2010a. Responses of snowmelt runoff to climatic change in an inland river basin, Northwestern China, over the past 50 years. *Hydrology and Earth System Sciences*, 14(10): 1979-1987.

Wang, J. and Li, S., 2005. The influence of climate change on snowmelt runoff variation in arid alpine regions of China. *Science in China (In Chinese)*, 35(7): 664-670.

Wang, J. and Li, W., 2001. Establishing snowmelt runoff simulating model using remote sensing data and GIS in the west of China. *International Journal of Remote Sensing*, 22(17): 3267-3274.

Wang, K., Wang, P., Li, Z., Cribb, M. and Sparrow, M., 2007. A simple method to estimate actual evapotranspiration from a combination of net radiation, vegetation index, and temperature. *Journal of Geophysical Research-Atmospheres*, 112(D15): D15107.

Wang, L., Caylor, K.K., Villegas, J.C., Barron-Gafford, G.A., Breshears, D.D. and Huxman, T.E., 2010b. Partitioning evapotranspiration across gradients of woody plant cover: Assessment of a stable isotope technique. *Geophysical Research Letters*, 37: L09401.

Wang, R., Yao, Z., Liu, Z., Wu, S., Jiang, L. and Wang, L., 2015. Snow cover variability and snowmelt in a high-altitude ungauged catchment. *Hydrological Processes*, 29(17): 3665-3676.

Wang, Y.-J. and Qin, D.-H., 2017. Influence of climate change and human activity on water resources in arid region of Northwest China: An overview. *Advances in Climate Change Research*, 8(4): 268-278.

Wei, X., Li, Q., Zhang, M., Giles-Hansen, K., Liu, W., Fan, H., Wang, Y., Zhou, G., Piao, S. and Liu, S., 2018. Vegetation cover-another dominant factor in determining global water resources in forested regions. *Global Change Biology*, 24(2): 786-795.

Wu, C., Hu, B.X., Huang, G. and Zhang, H., 2017. Effects of climate and terrestrial storage on temporal variability of actual evapotranspiration. *Journal of Hydrology*, 549: 388-403.

Wu, F., Zhan, J., Wang, Z. and Zhang, Q., 2015. Streamflow variation due to glacier melting and climate change in upstream Heihe River Basin, Northwest China. *Physics and Chemistry of the Earth*, 79-82: 11-19.

Xu, C.Y. and Singh, V.P., 2005. Evaluation of three complementary relationship evapotranspiration models by water balance approach to estimate actual regional evapotranspiration in different climatic regions. *Journal of Hydrology*, 308(1-4): 105-121.

Xu, T., Guo, Z., Liu, S., He, X., Meng, Y., Xu, Z., Xia, Y., Xiao, J., Zhang, Y. and Ma, Y., 2018. Evaluating Different Machine Learning Methods for Upscaling

Evapotranspiration from Flux Towers to the Regional Scale. *Journal of Geophysical Research: Atmospheres*, 123: 8674-8690.

Xu, X., Liu, W., Scanlon, B.R., Zhang, L. and Pan, M., 2013. Local and global factors controlling water-energy balances within the Budyko framework. *Geophysical Research Letters*, 40(23): 6123-6129.

Yang, D., Shao, W., Yeh, P.J.F., Yang, H., Kanae, S. and Oki, T., 2009. Impact of vegetation coverage on regional water balance in the nonhumid regions of China. *Water Resources Research*, 45: W00A14.

Yang, D.W., Sun, F.B., Liu, Z.T., Cong, Z.T. and Lei, Z.D., 2006. Interpreting the complementary relationship in non-humid environments based on the Budyko and Penman hypotheses. *Geophysical Research Letters*, 33(18): L18402.

Yang, H.B., Yang, D.W., Lei, Z.D. and Sun, F.B., 2008. New analytical derivation of the mean annual water-energy balance equation. *Water Resources Research*, 44(3): W03410.

Yang, L., Feng, Q., Yin, Z., Wen, X., Si, J., Li, C. and Deo, R.C., 2017. Identifying separate impacts of climate and land use/cover change on hydrological processes in upper stream of Heihe River, Northwest China. *Hydrological Processes*, 31(5): 1100-1112.

Yang, T., Wang, C., Chen, Y., Chen, X. and Yu, Z., 2015. Climate change and water storage variability over an arid endorheic region. *Journal of Hydrology*, 529: 330-339.

Ye, S., Li, H.Y., Li, S., Leung, L.R., Demissie, Y., Ran, Q. and Blöschl, G., 2016. Vegetation regulation on streamflow intra-annual variability through adaption to climate variations. *Geophysical Research Letters*, 42(23): 10307-10315.

Yuan, W., Liu, S., Liu, H., Randerson, J.T., Yu, G. and Tieszen, L.L., 2010. Impacts of precipitation seasonality and ecosystem types on evapotranspiration in the Yukon River Basin, Alaska. *Water Resources Research*, 46: W02514.

Zeng, R. and Cai, X., 2015. Assessing the temporal variance of evapotranspiration considering climate and catchment storage factors. *Advances in Water Resources*, 79: 51-60.

Zeng, R. and Cai, X., 2016. Climatic and terrestrial storage control on evapotranspiration temporal variability: Analysis of river basins around the world. *Geophysical Research Letters*, 43(1): 185-195.

Zha, T., Barr, A.G., van der Kamp, G., Black, T.A., McCaughey, J.H. and Flanagan, L.B., 2010. Interannual variation of evapotranspiration from forest and grassland ecosystems in western canada in relation to drought. *Agricultural and Forest Meteorology*, 150(11): 1476-1484.

Zhang, D., Cong, Z., Ni, G., Yang, D. and Hu, S., 2015. Effects of snow ratio on annual runoff within the Budyko framework. *Hydrology and Earth System Sciences*, 19(4): 1977-1992.

Zhang, D., Liu, X., Zhang, Q., Liang, K. and Liu, C., 2016a. Investigation of factors affecting intra-annual variability of evapotranspiration and streamflow under different climate conditions. *Journal of Hydrology*, 543: 759-769.

Zhang, D., Liu, X., Zhang, L., Zhang, Q., Gan, R. and Li, X., 2020. Attribution of Evapotranspiration Changes in Humid Regions of China from 1982 to 2016. *Journal of Geophysical Research-Atmospheres*, 125(13): e2020JD032404.

Zhang, L., Dawes, W.R. and Walker, G.R., 2001. Response of mean annual evapotranspiration to vegetation changes at catchment scale. *Water Resources Research*, 37(3): 701-708.

Zhang, S., Yang, H., Yang, D. and Jayawardena, A.W., 2016b. Quantifying the effect of vegetation change on the regional water balance within the Budyko framework. *Geophysical Research Letters*, 43(3): 1140-1148.

Zhang, Y., Luo, Y., Sun, L., Liu, S., Chen, X. and Wang, X., 2016c. Using glacier area ratio to quantify effects of melt water on runoff. *Journal of Hydrology*, 538: 269-277.

Zhou, S., Yu, B., Huang, Y. and Wang, G., 2015. The complementary relationship and generation of the Budyko functions. *Geophysical Research Letters*, 42(6): 1781-1790.